Imperial College
London

Planning Report for MSc Project

Automated segmentation of spine and soft tissue in the torso for spine modelling in CT

Author name: Huijing Zhou

Supervisor: Dr Spyros Masouros

Monday, 01 March 2021

Word count: 3845

1. Project Specification

Spine and soft tissue segmentation from medical images is a key step in the process of biomechanical modelling, such as finite element model[1] and multi-body model[2]. It contributes by calculating the masses and rotations needed in multi-body model analysis particularly. And this model facilitates the study of spinal biomechanics, such as gait analysis[3]. In addition, it can be applied to the treatment and assessment of spinal disorders, which is regarded as a key technique for non-invasive surgical planning and navigation[4].

Segmentation and calculation of spine and soft tissue for reconstruction of spine images have mostly been done manually in CT scans using software such as MIMICS or ImageJ[2]. Taking MIMICS as an example, the tissues in each 2D slice need to be manually segmented, and then the 3D segmentation can be completed by stacking slices. This method is time-consuming especially when facing a large dataset (The number of transverse CT scans of each person's upper body usually exceeds 1000).

Therefore, researchers have developed automated segmentation algorithms for different tissues in CT scans. However, most of them focus on specific tissue (fat, muscles, bones, etc.) [5-11]. Due to the close connection and small contrast difference between the target tissue and others, these algorithms are much more complex and usually with a long-running time, which may overfit the spine and soft tissue segmentation. Therefore, to generate a multi-body model of the spine, an automated and simpler segmentation method for spine and soft tissue is needed.

The project aims to develop an automated image processing tool for calculating vertebral volumes and its 3D geometric centroids. This will be realised by segmenting the spine and soft tissue region in transverse slices. Then it will combine with the previous research on vertebral body heights (VBHs) in sagittal and coronal slices done previously (unpublished work), in order to calculate the segmental torso volumes and centroids.

2. Ethical Analysis

Three cadavers' complete upper body CT scans will be used as research objects in this project. All the data collection procedures were carried about by researchers in the University of Virginia (UVA) and they were approved by the UVA Cadaver Use Committee. Necessary informed consent from three cadavers and/or the support of their families were obtained before data collection, in order to ensure the legality of using the data. Moreover, the data was collected by using "GE MEDICAL SYSTEM" under the operation of professional radiologists, in order to ensure the accuracy of data measurement.

Developing an automated algorithm for the segmentation of the spine and soft tissue for building the spine model has long-term significance in both research and clinics. From the research perspective, it speeds up the calculation and improves the segmentation accuracy compared to manual marking. It also helps researchers to study biomechanical effects, such as the mechanical relationship between the vertebrae as well as between vertebrae and muscles[12], which promotes the research on various spinal diseases (such as spine deformation). Clinically, with automatic processing, doctors can evaluate the medical conditions of patients faster and make a quicker and better surgical plan using the spine virtual model[13]. Besides, automated segmentation and modelling can help doctors improve pedicle screw insertion accuracy (a widely used treatment method in spinal surgeries), which can increase the success rate of surgeries and the cure rate of patients[14-16].

This evaluated automated algorithm is applicable to the volume and centroid extraction based on the multi-body model for spine modelling. Prior to clinical applications, segmentation and spine modelling results should be re-evaluated for specific patient's CT dataset. Once the evaluation requirements are met, the experienced radiologists or doctors are responsible for giving clinical and surgical advice, in order to minimise surgical errors due to the misuse of the algorithm.

3. Literature Review

Several studies have used semi-automatic methods to extract parameters for spine modelling[2 17-19]. Keenan et al. used the "Segmented Line" tool in ImageJ to draw the contours of each target region of transverse slices, completing the calculation of their area and centroids[2]. Rehm et al. used the EOS imaging system for modelling, which required sterEOS software-trained radiologists to mark the primary vertebral anatomic landmarks[17]. However, the marking process is always regarded as a time-consuming part. Pomero et al. spent an average of 14 min 20 s finishing spine reconstruction using a combined geometric and statistic model, and most of the time was spent on marking[18]. Besides, this method required fine adjustments of the vertebral shape, bringing the reconstruction time up to 20 min[19], which was not practical for some clinical applications. In order to solve the time-consuming problem caused by manually marking, Humbert et al. proposed a novel semi-automatic method using parametric models based on transversal and longitudinal inferences to reduce the number of anatomic landmarks[19]. The mean reconstruction time was 10 min for completing verification of the whole vertebral shape[19]. However, the time that this method can reduce is still limited. Therefore, replacing the marking process with an automated method to speed up the spine modelling is necessary.

Some researchers have investigated automated segmentation algorithms to detect the spine and soft tissue regions[5-11].

For spine segmentation, Liu segmented the vertebral bodies (VBs) by drawing rays from the VB centroids and retained the interactions between rays and the high confidence boundary of VB images[5]. Those interactions were used to outline VBs based on dynamic attraction map[5]. The overall Dice similarity coefficient (DSC) was 0.939[5]. Besides, some researchers have segmented VBs depending on prior shape[6 7]. Stern initialised each VB as an elliptical cylinder and deformed that by modifying parameters of a 3D superquadric model[6]. Aslan used graph cut with the linear combination of Gaussians (LCG) and Markov Gibbs Random Field (MGRF) to fit the VB shape after comparing the initial VB segmentation done by matched filter with the 3D VB shape obtained from other databases[7]. The average error of this method was 4.9% and the average running time was 7.1 s per 10 slices[7].

For soft tissue detection, a simpler method is to subtract the area of the body cavities from the area of the torso. For torso outline detecting, this could be transformed into detecting subcutaneous adipose tissue (SAT) outline. Popuri completed fat tissue segmentation of 1000 abdominal CT and 530 chest CT, based on finite element method (FEM) deformable model that combined with prior shape information via a statistical deformation model (SDM), with a Jaccard coefficient exceeding 90%[8]. For detecting cavities, Than et al. used Otsu grey level thresholding and morphological filtering for initial lung extraction, then applied Radon transform and accumulating the pixel width to segment the left and right lung regions[9]. The success rate was 79.0% for the right lung and 92.6% for the left lung[9]. Nithila et al. used selective binary and Gaussian filtering with a new signed pressure force function (SBGF-new SPF) for lung parenchyma detection[10]. And then Fuzzy C-Mean (FCM) clustering was used to separate the internal structures from lung[10]. Dai et al. finished the segmentation using an improved graph cuts algorithm combined with Gaussian Mixture Model (GMM), with a DSC of 98.74% and 10 - 15 min running time[11].

For removing metal artefacts, there are mainly two categories of methods: projection completion based methods and statistically based iterative methods[20]. For the former one, the metal projections are treated as missing data that can be completed by interpolations[20]. Mahnken et al. proposed a threshold-based interpolation algorithm. A threshold was set to segment the metal objects, and the interpolated values, as well as corresponding weights, were applied to do the correction[21]. In the latter case, it assumes metal artefacts are mainly caused by noise, beam hardening, scattering, partial volume effects and blending so that algorithms to model the noise, the beam hardening, etc. have become a way to reduce metal artefacts[22]. Bal et al. used tissue-class modelling and adaptive prefiltering, and the results showed

that the mean Hounsfield units for tissue and bone varied less than 1% and 2%[23]. Boas compared the metal deletion technique (MDT), one of the iterative methods, with linear interpolation (LI). Their average error did not differ much (90 HU and 154 HU respectively). However, 28 min was required to process one slice with MDT, while only 3.1 minutes with LI[24].

There are many image segmentation algorithms for tissue extraction, but most of them are suitable for specific tissue (fat, muscles, bones, etc.) with more parameters to be set, strong algorithmic complexity, as well as long-running time. Meanwhile, the algorithms do not involve arms and the CT bed removal, which means they may not be suitable for spine modelling. Therefore, it is necessary to develop a fast and suitable automated algorithm for vertebral-parameter calculation.

4. Implementation Plan

4.1. Extraction of the transverse slices to be processed

In the previous study (unpublished work), Tan completed the manual masking of VBs in the sagittal and coronal planes and extracted their VBHs using 4 automated methods. The centroid coordinates of vertebrae were extracted during the process of method 4 using the "centroid" function in MATLAB. The transverse slices through those centroids will be exported as the target slices to be processed and calculated. This results in 24 transverse slices of the vertebrae (from C1 to T5) per subject. The vertebrae for this study do not include sacrum or coccyx because the method of calculating volumes and centroids used in this study assumes the objects are columnar homogeneous.

4.2. Segmentation of soft tissue (including arms and the CT bed)

Segmentation of soft tissue region including arms and the CT bed (shown in Figure 1 (a)) can be obtained by firstly segmenting the region of torso including arms and the CT bed (shown in Figure 1 (b)), and then removing the region of cavities such as lung parenchyma, gas in stomach or abdomen, etc. As the Hounsfield units (HU) of background and cavities to be removed differs significantly from that of soft tissue (the higher Hounsfield units, the brighter the pixel tends to be), the global thresholding method combined with morphological transformation will be used to complete the initial segmentation (including arms and the CT bed), which is a simple and fast method of separating the background and the objects by setting one threshold overall. Then the results will be optimised by region growing and graph cut.

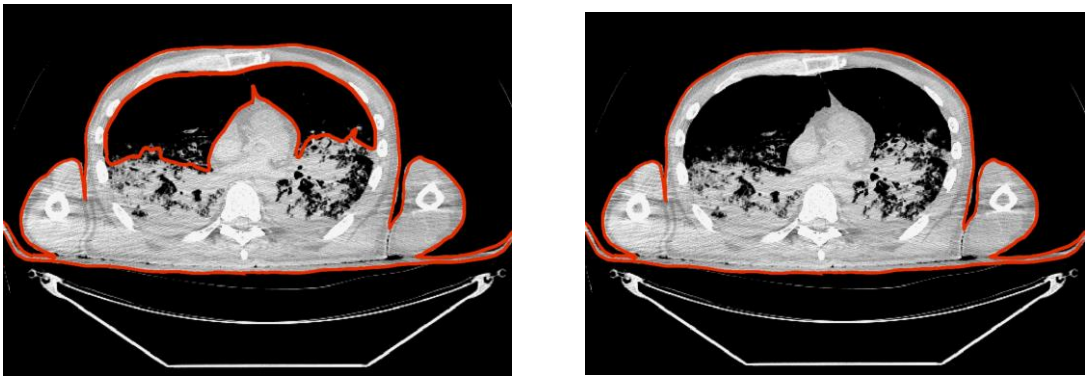

(a) (b)

Figure 1: Transverse slice through the centroid of 8th thoracic vertebra in subject 00606M. (a) Torso with cavities removed masked in red. (b) Torso including arms and the CT bed masked in red.

4.3. The CT bed and subjects' arms removal

The projections of the CT bed (shown in Figure 2 (a)) and arms (show in Figure 2 (b)) need to be removed because arms are attached to the shoulders, not directly to the trunk, while the CT bed is not part of the body. Otherwise, they would change the volume and centroid calculation.

Due to the close connection between the CT bed, arms and torso, edge detection algorithms and watershed algorithm combined with morphological transformation will be applied to realise the segmentation and removal of arms and the CT bed from the torso.

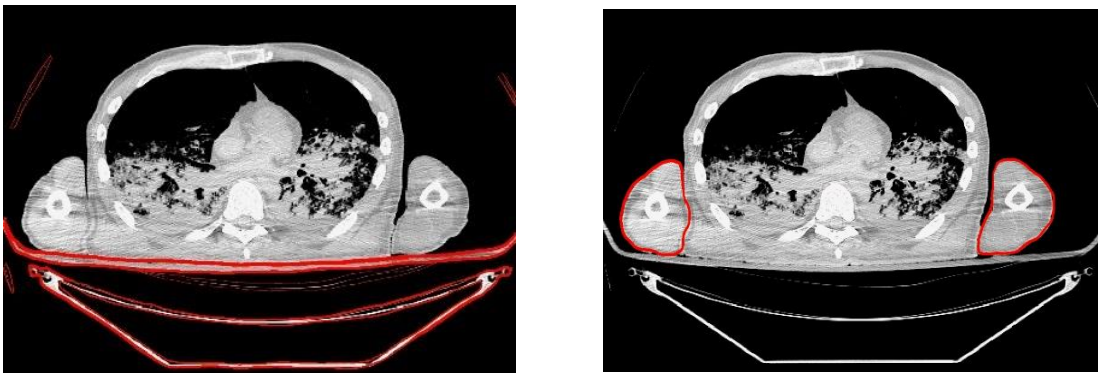

(a) (b)

Figure 2: Transverse slice through the centroid of 8th thoracic vertebra in subject 00606M. (a) The CT bed region masked in red. (b) Arms region masked in red.

4.4. Metal artefacts removal

Metallic substances implanted in the human body (such as pacemakers, dentures, prosthetic joints, etc.) may cause metal artefacts in CT images. These metal objects have a stronger ability to absorb photons than human tissues, so it appears as a light spot on the CT images and generates a shadow around it[25], as shown in Figure 3. Those will affect image quality by reducing contrast and occluding details, which will also lead to mis-segmentation of some pixels. In order to remove those, the linear interpolation (LI) method of reprojecting the metal trajectory will be applied in this step.

Figure 3: Metal artefacts in CT scans.

4.5. Segmentation of vertebral bodies

Due to the big Hounsfield units difference between the spine and other tissue, the global thresholding method will be applied to separate them. Then the initial VB region can be regarded as its

maximum connectivity area. Graph cut or matched filter can be applied here to get the VB region (shown in Figure 4), combining with the prior spine shape information which initially regards the VB as a circle.

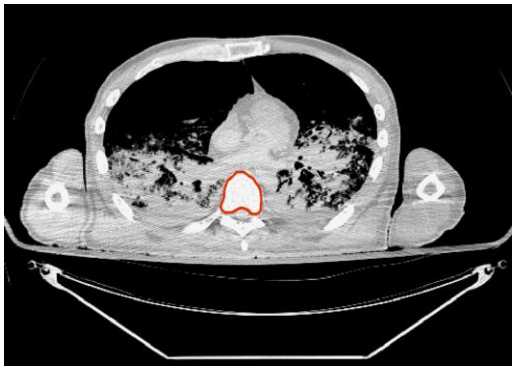

Figure 4: Transverse slice through the centroid of 8th thoracic vertebra in subject 00606M. Vertebral body region in CT masked in red.

4.6. Batch image processing and algorithm optimisation

In order to complete automated segmentation of all extracted 72 axial slices, automated parameter setting should be realised, as the parameters (such as the global threshold) may differ from different parts of the body and different subjects. Ostu method and adaptive threshold method will be applied in this step to realise automated threshold setting.

4.7. Segmental torso volume and centroid calculation

Keenan et al. proposed segmental torso volume and centroid estimation method using the vertebral body height and the central slice area[2]. Then based on the above experimental results on the central slice area and previous research done in the Bioengineering Department on vertebral body heights by Tan (unpublished yet), segmental torso volumes and centroids will be calculated in this step.

4.8. Project timetable

Project Milestones	DEC	JAN	FEB	MAR	APR	MAY	JUN	JUL	AUG	SEP
Literature Review	→									
Transverse slices extraction		→								
Torso segmentation			→							
Cavities segmentation			→							
The CT bed removal				→						
Arms removal				→						
Exam break					→					
Metal artefacts removal						→				
VBs segmentation							→			
Evaluation of accuracy								→		
Volumes and centroids calculation								→		
Optimisation								→		
Write up									→	

Table 1: Monthly implantation plan of the project.

4.9. Backup plan

If the segmentation cannot be successfully implemented due to the limitations of algorithms, building deep learning networks such as CNN, U-Net etc. will be considered to segment soft tissue, arms, the CT bed and spine. As this project does not involve the extraction of tissues from specific parts of the body (lungs, abdomen, brain, etc.), each labelled slice can be used as a sample for training and testing. For this project, more than 3000 samples in total can be used to train the artificial intelligence model, which can be regard as a sufficient amount of data. Another method is to use other databases that are already labelled for training and testing. The generated model can be applied to three cadavers' datasets for further testing since the model should be generic to all datasets for the same detected objects.

5. Risk register

Risk	Risk description	Probability	Severity	Risk	Mitigating Action
Computer crash	This project is desk-based and all experiments, as well as papers, need to be completed on the computer. The computer crash will have a serious impact on project progress.	1	4	4	1. Clean up unused or temp files. 2. Complete complicated calculation work on the remote desktop.
Data loss	The loss of data (including but not limited to the original CT scans, literature, codes, experimental results, reports) will influence project progress.	2	5	10	1. Backup files in at least 3 places (computer hard disk, external hard disk, Onedrive, etc.). 2. Organize experimental codes and data regularly.
Time management	In order to finish 2 object detection and 3 interference removal, many algorithms worth trying, which may be time-consuming.	2	2	4	1. Strictly follow the project timetable. 2. Meet with supervisor regularly.
Ineffective algorithms	Due to the database particularity or algorithm limitations, the target objects cannot be segmented successfully using selected algorithms. This will lead to a waste of time and may cause lagging experimental progress.	2	4	8	1. Report the project progress each week. 2. Communicate current problems with supervisor each week.
MIMICS license expiry	Due to software version or licence problems, MIMICS may not be successfully activated, or some functions may not be available. Meanwhile, the licence provided by the Department has an expiry date.	2	1	2	1. Contact customer service. 2. Communicate with the supervisor. 3. Export all the CT data in DICOM format in advance. 4. Try to finish all the work in MIMICS before the licence expires.

Table 2: Risk register table of the project.

			Severity				
			Catastrophic	**Critical**	**Serious**	**Minor**	**Negligible**
			5	4	3	2	1
Likelihood	**Frequent**	5	25	20	15	10	5

	Probable	4	20	16	12	8	4
	Occasional	3	15	12	9	6	3
	Remote	2	10	8	6	4	2
	Improbable	1	5	4	3	2	1

Table 3: Risk management heat map (5x5) showing likelihood and severity.

6. Evaluation plan

6.1. Manual mask drawing of the spine and soft tissue

As there is no reference for the spine and soft tissue regions, the accuracy of this automated algorithm will be compared with the manually spine and soft tissue masks. Three slices from each of the cervical spine, thoracic spine and lumbar spine respectively will be masked by three observers who have the bioengineering/spine modelling background through MIMICS. Then perimeter, area and centroids of those masked slices will be calculated automatically using the "Measure" tool in MIMICS.

6.2. Inter-observer reliability of perimeter area and centroids

The intraclass correlation coefficient (ICC) will be applied to measure the inter-observer reliability for parameters (perimeters area and centroids) obtained in 6.1 after three observers' masking. The ICC of each parameter among the 3 observers will be calculated separately. The inter-observer reliability can consider being good if all their ICCs are greater than 0.75.

6.3. Accuracy of the spine and soft tissue segmentation

In order to evaluate the performance of this automated segmentation algorithm, the Dice similarity coefficient (DSC) will be used, which is the most commonly used indicator in image segmentation[26]. It is an overlap-based indicator and it quantitatively describes the intersection of two data sets, by normalizing the size of their intersection over the average of their sizes. And if DSC is closer to 1, the segmentation effect is better. The formula is as follows:

$$DSC = \frac{2|X \cap Y|}{|X| + |Y|}$$

Where in this project, X is the torso (not including arms) area minus the soft tissue area obtained based on the automatic segmentation algorithm developed in this project, and Y is the ground truth resulted from manual segmentation.

6.4. Evaluation of volume and centroid calculation

McConville et al. have completed 75 body volume and centroid variables measurements of the total body of cadavers based on easily located body landmarks[27]. The automated calculated volumes and centroids will be compared with the values mentioned in McConville's research.

7. Preliminary Results

7.1. Preparation

Literature reading, software downloading and testing, as well as database analysis, have been completed.

Literature study and review on spine modelling, CT image segmentation and metal artefacts removal have been finished to gain an in-depth understanding of its principles and methods.

The project will be mainly based on Python 3.8 and OpenCV2 for image segmentation and MIMICS 23.0 for the selection of target transverse slices as well as the drawing of masks for evaluation. The software has been installed and activated and the programming environment has been set up.

This database includes three subjects' (all male) complete upper body CT scans. There are more than 1000 clear transverse slices for each subject and each of those slices is a grayscale image with 16 grayscales and a size of 512*512. The slice thickness for two subjects (00606M and 00636M) is 0.6250mm while the thickness of another subject (00525M) is 1.2500mm. Besides, it can be distinguished from the transverse CT slices of the subject (00636M) that there are metal artefacts.

7.2. Extraction of CT transverse slices through vertebral body centroids

The initial VB centroid coordinates from 1st cervical (C1) to 5th lumbar vertebra (T5) of 3 subjects were extracted by calculating the proportion of the extracted longitudinal coordinates to the entire image then multiplying by the maximum acquisition height of each subject. The closest values to those initial coordinates were found in the bottom right corner of the MIMICS Axial Slice Display Window, corresponding to the slices used for calculating the area. The slice number (counted from bottom to top) was calculated by dividing the closest values by the slice thickness. And Table 4 shows the slice number result of each subject.

Slice number	**C1**	**C2**	**C3**	**C4**	**C5**	**C6**
00606M	Nah	1246	1228	1197	1167	1139
00636M	Nah	Nah	Nah	Nah	Nah	Nah
00526M	1079	1058	1022	990	962	937
	C7	**T1**	**T2**	**T3**	**T4**	**T5**
00606M	1113	1084	1053	1023	989	955
00636M	Nah	Nah	Nah	1033	1000	963
00526M	912	884	854	823	786	748
	T6	**T7**	**T8**	**T9**	**T10**	**T11**
00606M	916	879	841	801	761	716
00636M	927	890	852	814	773	730
00526M	709	668	628	585	540	492
	T12	**L1**	**L2**	**L3**	**L4**	**L5**
00606M	668	619	568	513	460	405
00636M	685	637	586	538	486	431
00526M	442	390	329	268	208	148

Table 4: The slice number of three subjects' each vertebra. "Nah" represents the previous study done by the department that has not covered this vertebra.

7.3. Torso (including arms and partial CT bed) segmentation

The global thresholding method and morphological transformations were used to segment the initial torso. After threshold setting, the background value was set to False (zero) while the object value was set to True (one), where a binary image was obtained. Then closing (one of the morphological transformations) with a circular structural unit was used to remove part of the CT bed area and also some spots which may influence contour detection. Following filling all the holes, the mask and the contour of the torso (with arms and partial CT bed) could be obtained.

The transverse slice corresponding to the 8th thoracic vertebra of subject 00606M was chosen to test the code. The global threshold was manually set to 800, and the radius of the circular structural unit was set to 3 pixels. The initial segmentation result shows in Figure 5.

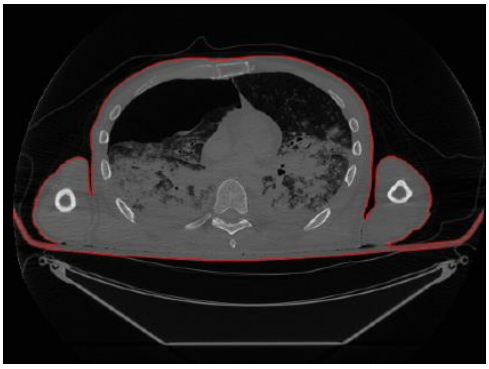

Figure 5: Initial torso (including arms and partial CT bed) segmentation of 8th thoracic vertebra in subject 00606M, using the global thresholding and morphological transformations.

7.4. Cavity segmentation

Based on the results in 7.3, the images before and after the removal of holes were subtracted to obtain the initial cavity region (lung parenchyma for this case). Then small connected objects were removed to obtain the mask of the complete cavity region. Finally, the soft tissue mask could be acquired by subtracting the torso mask from the cavity mask.

The same transverse slice in 7.3 was used to test the code, as it includes a relatively larger area of the lung parenchyma, which makes it easier to show the results of the soft tissue segmentation. The smallest allowable connected object size was set to 300 pixels. The segmentation results of the cavity as well as soft tissue show in following Figure 6.

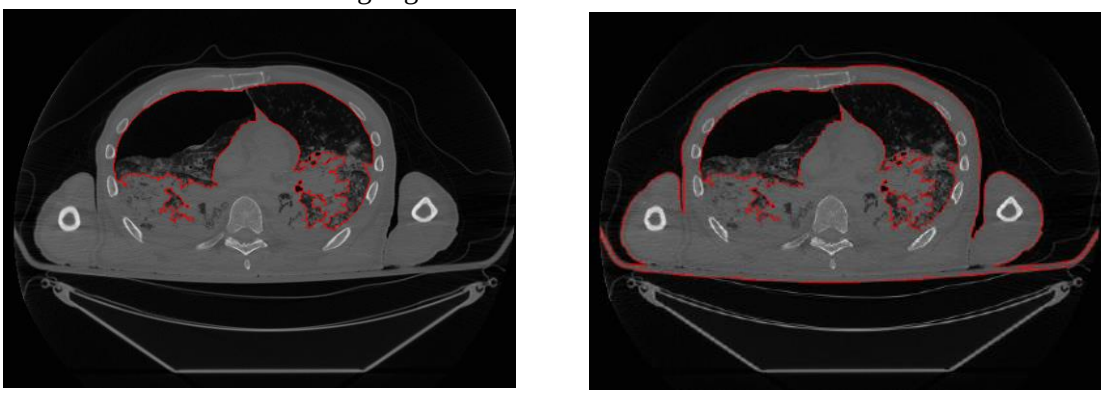

(a) (b)

Figure 6: (a) Cavity segmentation of 8th thoracic vertebra (T8) in subject 00606M. (b) Soft tissue segmentation of 8th thoracic vertebra (T8) in subject 00606M.

7.5. Summary of preliminary results

The test results above indicate that the global thresholding method combined with morphological transformations can segment the soft tissue. However, it requires the manual threshold setting and is not able to remove the arms nor all the CT bed, which needs further optimisation.

8. References

1. Jalalian A, Gibson I, Tay E H. Computational biomechanical modeling of scoliotic spine: challenges and opportunities[J]. Spine Deformity, 2013, 1(6): 401-411.
2. Keenan B E, Izatt M T, Askin G N, et al. Segmental torso masses in adolescent idiopathic scoliosis[J]. Clinical Biomechanics, 2014, 29(7): 773-779.
3. De Groote F, De Laet T, Jonkers I, et al. Kalman smoothing improves the estimation of joint kinematics and kinetics in marker-based human gait analysis[J]. Journal of biomechanics, 2008, 41(16): 3390-3398.
4. Little J P, Adam C. Towards determining soft tissue properties for modelling spine surgery: current progress and challenges[J]. Medical & biological engineering & computing, 2012, 50(2): 199-209.
5. Liu S, Xie Y, Reeves A P. Automated 3D closed surface segmentation: application to vertebral body segmentation in CT images[J]. International journal of computer assisted radiology and surgery, 2016, 11(5): 789-801.
6. Štern D, Likar B, Pernuš F, et al. Parametric modelling and segmentation of vertebral bodies in 3D CT and MR spine images[J]. Physics in Medicine & Biology, 2011, 56(23): 7505.
7. Aslan M S, Ali A, Farag A A, et al. 3d vertebral body segmentation using shape based graph cuts[C]//2010 20th International Conference on Pattern Recognition. IEEE, 2010: 3951-3954.
8. Popuri K, Cobzas D, Esfandiari N, et al. Body composition assessment in axial CT images using FEM-based automatic segmentation of skeletal muscle[J]. IEEE transactions on medical imaging, 2015, 35(2): 512-520.
9. Than J C M, Noor N M, Rijal O M, et al. Lung segmentation for HRCT thorax images using radon transform and accumulating pixel width[C]//2014 IEEE Region 10 Symposium. IEEE, 2014: 157-161.
10. Nithila E E, Kumar S S. Segmentation of lung nodule in CT data using active contour model and Fuzzy C-mean clustering[J]. Alexandria Engineering Journal, 2016, 55(3): 2583-2588.
11. Dai S, Lu K, Dong J, et al. A novel approach of lung segmentation on chest CT images using graph cuts[J]. Neurocomputing, 2015, 168: 799-807.
12. Tesh K M, Dunn J S, Evans J H. The abdominal muscles and vertebral stability[J]. Spine, 1987, 12(5): 501-508.
13. Chua C K, Chou S M, Lin S C, et al. Rapid prototyping assisted surgery planning[J]. The International Journal of Advanced Manufacturing Technology, 1998, 14(9): 624-630.
14. Tian N F, Huang Q S, Zhou P, et al. Pedicle screw insertion accuracy with different assisted methods: a systematic review and meta-analysis of comparative studies[J]. European Spine Journal, 2011, 20(6): 846-859.
15. Su P, Zhang W, Peng Y, et al. Use of computed tomographic reconstruction to establish the ideal entry point for pedicle screws in idiopathic scoliosis[J]. European Spine Journal, 2012, 21(1): 23-30.
16. Elmi-Terander A, Burström G, Nachabé R, et al. Augmented reality navigation with intraoperative 3D imaging vs fluoroscopy-assisted free-hand surgery for spine fixation surgery: a matched-control study comparing accuracy[J]. Scientific reports, 2020, 10(1): 1-8.
17. Rehm J, Germann T, Akbar M, et al. 3D-modeling of the spine using EOS imaging system: Inter-reader reproducibility and reliability[J]. PLoS One, 2017, 12(2): e0171258.
18. Pomero V, Mitton D, Laporte S, et al. Fast accurate stereoradiographic 3D-reconstruction of the spine using a combined geometric and statistic model[J]. Clinical Biomechanics, 2004, 19(3): 240-247.

19. Humbert L, De Guise J A, Aubert B, et al. 3D reconstruction of the spine from biplanar X-rays using parametric models based on transversal and longitudinal inferences[J]. Medical engineering & physics, 2009, 31(6): 681-687.
20. Lemmens C, Faul D, Nuyts J. Suppression of metal artifacts in CT using a reconstruction procedure that combines MAP and projection completion[J]. IEEE transactions on medical imaging, 2008, 28(2): 250-260.
21. Mahnken A H, Raupach R, Wildberger J E, et al. A new algorithm for metal artifact reduction in computed tomography: in vitro and in vivo evaluation after total hip replacement[J]. Investigative radiology, 2003, 38(12): 769-775.
22. De Man B, Nuyts J, Dupont P, et al. Metal streak artifacts in X-ray computed tomography: a simulation study[J]. IEEE Transactions on Nuclear Science, 1999, 46(3): 691-696.
23. Bal M, Spies L. Metal artifact reduction in CT using tissue‐class modeling and adaptive prefiltering[J]. Medical physics, 2006, 33(8): 2852-2859.
24. Boas F E, Fleischmann D. Evaluation of two iterative techniques for reducing metal artifacts in computed tomography[J]. Radiology, 2011, 259(3): 894-902.
25. Pauwels R, Stamatakis H, Bosmans H, et al. Quantification of metal artifacts on cone beam computed tomography images[J]. Clinical oral implants research, 2013, 24: 94-99.
26. Skourt B A, El Hassani A, Majda A. Lung CT image segmentation using deep neural networks[J]. Procedia Computer Science, 2018, 127: 109-113.
27. McConville J T, Clauser C E, Churchill T D, et al. Anthropometric relationships of body and body segment moments of inertia[R]. ANTHROPOLOGY RESEARCH PROJECT INC YELLOW SPRINGS OH, 1980.